



VCU

Virginia Commonwealth University
VCU Scholars Compass

Theses and Dissertations


Graduate School

2019

RESONANT ACOUSTIC WAVE ASSISTED SPIN-TRANSFER-TORQUE SWITCHING OF NANOMAGNETS

Austin R. Roe
Virginia Commonwealth University

Follow this and additional works at: <https://scholarscompass.vcu.edu/etd>

 Part of the [Electronic Devices and Semiconductor Manufacturing Commons](#), [Nanoscience and Nanotechnology Commons](#), and the [Other Mechanical Engineering Commons](#)

© The Author

Downloaded from

<https://scholarscompass.vcu.edu/etd/6029>

This Thesis is brought to you for free and open access by the Graduate School at VCU Scholars Compass. It has been accepted for inclusion in Theses and Dissertations by an authorized administrator of VCU Scholars Compass. For more information, please contact libcompass@vcu.edu.

RESONANT ACOUSTIC WAVE ASSISTED SPIN-TRANSFER-TORQUE SWITCHING OF NANOMAGNETS

A thesis submitted in partial fulfilment of the requirements for the degree of Master of Science at
the Virginia Commonwealth University.

By

Austin Reid Roe

Bachelor of Science in Mechanical Engineering, Virginia Military Institute, 2017.

Director: Jayasimha Atulasimha,

Professor, Department of Mechanical and Nuclear Engineering

Virginia Commonwealth University

Richmond, Virginia

August, 2019

Acknowledgement

My research would not have been possible without the aid and support of my advisor, Dr. Jayasimha Atulasimha. His assistance starting before I even began the graduate program and all throughout my research and graduate studies allowed me to push further than I thought and get to where I am now. I am very grateful to have had this excellent mentor be a part of my academic career and I look forward to what I will further be able to accomplish thanks to the personal and professional growth that I was able to achieve with his guidance.

I would also like to thank my thesis committee, Dr. Supriyo Bandyopadhyay and Dr. Ravi Hadimani, for their invaluable input and feedback on my thesis to help make it what it is now.

I give my gratitude to Dhritiman Bhattacharya, Md Ali Azam, and my other lab mates, peers, and colleagues at VCU as well the tremendous staff of the VCU School of Engineering. You have aided and supported me in too many ways to describe.

I acknowledge the time spent and the valuable experience gained from my internship at the Naval Research Lab (NRL) during my graduate program, I would like to specifically thank Dr. Scott Mathews for his help and guidance.

I acknowledge the academic and financial support from the VCU School of Engineering and the National Science Foundation NSF SHF Small grant CCF-1815033.

Finally, and most importantly, I give my thanks to my friends and family. My parents, Reid and Sherry Roe, made me the person I am today, and I will always look up to them and am proud to be their son. I cannot thank the rest of my family and friends enough for their unconditional love, support, and encouragement, I could not have made it this far without them.

Table of Contents

List of Tables	iv
List of Figures	iv
Abstract	vi
Chapter 1: Introduction	1
1.1 Non-Volatile RAM.....	1
1.2 Switching Schemes.....	2
1.3 Scaling Issues with Strain.....	5
1.4 Motivation for Combined Resonant SAW and STT.....	6
Chapter 2: Combined Resonant SAW and STT switching of p-MTJs	8
2.2 Modelling Approach.....	9
2.3 In-Plane Switching with SAW and STT.....	11
2.4 Thermal Noise.....	13
2.5 Out-of-Plane Switching with SAW and STT.....	14
2.6 Out-of-Plane Switching Energy Comparison.....	16
Chapter 3: Conclusion	18
References	19
Appendix	23

List of Tables

Table I: FeGa material properties.....	10
--	----

List of Figures

Figure 1.1: General structure of a magnetic tunnel junction.....	3
Figure 1.2: Straintronics switching with dipole coupling showing complete reversal of the magnetization.....	4
Figure 1.3: Difference in the deflection from the easy axis due to applied SAW of 11 and 11.25 GHz.....	7
Figure 2.1: (a) MTJ array switched with resonant SAW and STT (b) Magnetization dynamics with resonant SAW + STT switching of in-plane magnetization (c) Magnetization dynamics with resonant SAW + STT switching of out-of-plane magnetization.....	8
Figure 2.2: Magnetization dynamics of an in-plane nanomagnet with SAW illustrating the doubling of the applied frequency to resonate with one cycle of the motion of the magnetization.....	11
Figure 2.3: In-plane magnetization dynamics simulations with (a) no thermal noise, (b) resonant SAW and STT, and (c) STT only and no SAW. NOTE: Angle shown is the azimuthal angle φ with $\sim 90^\circ$ degree being the initial orientation and both $\sim 270^\circ$ and $\sim -90^\circ$ representing a successful switch, while return to $\sim 90^\circ$ degree being an unsuccessful switching event.....	12

Figure 2.4: Simulation of in-plane magnetization dynamics with thermal effects showing how thermal fluctuations affect timing of the application of the STT.....14

Figure 2.5: Out-of-plane magnetization dynamics simulations with (a) comparison of resonant SAW with and without thermal noise to purely thermal noise and (b) switching of out-of-plane magnetization with resonant SAW and STT (angle shown is the polar angle, θ) (c) Switching probability vs. STT current density of three different SAW magnitudes as well as for no SAW applied.....17

Abstract

Title of Dissertation: RESONANT ACOUSTIC WAVE ASSISTED SPIN-TRANSFER-TORQUE SWITCHING OF NANOMAGNETS

By Austin Reid Roe

A thesis submitted in partial fulfilment of the requirements for the degree of Master of Science at Virginia Commonwealth University.

Virginia Commonwealth University, 2019.

Major Director: Jayasimha Atulasimha, Professor, Department of Mechanical and Nuclear Engineering

We studied the possibility of achieving an order of magnitude reduction in the energy dissipation needed to write bits in perpendicular magnetic tunnel junctions (p-MTJs) by simulating the magnetization dynamics under a combination of resonant surface acoustic waves (r-SAW) and spin-transfer-torque (STT). The magnetization dynamics were simulated using the Landau-Lifshitz-Gilbert equation under macrospin assumption with the inclusion of thermal noise. We studied such r-SAW assisted STT switching of nanomagnets for both in-plane elliptical and circular perpendicular magnetic anisotropy (PMA) nanomagnets and show that while thermal noise affects switching probability in in-plane nanomagnets, the PMA nanomagnets are relatively robust to the effect of thermal noise. In PMA nanomagnets, the resonant magnetization dynamics builds over few 10s of cycles of SAW application that drives the magnetization to precess in a cone with a deflection of $\sim 45^\circ$ from the perpendicular direction. This reduces the STT current density required to switch the magnetization direction without increasing the STT application time

or degrading the switching probability in the presence of room temperature thermal noise. This could lead to a pathway to achieve energy efficient switching of spin-transfer-torque random access memory (STT-RAM) based on p-MTJs whose lateral dimensions can be scaled aggressively despite using materials with low magnetostriction by employing resonant excitation to drive the magnetization away from the easy axis before applying spin torque to achieve a complete reversal.

Chapter 1: Introduction

Random access memory (RAM) enables processors to store data for short-term, high-speed use. Specifically, RAM allows the computer processor to quickly pull (read) and store (write) data during computations. The most common type of RAM is dynamic RAM (DRAM) and comprises a transistor and a capacitor. These simple devices are relatively inexpensive and packed densely, leading to high capacity modules. DRAM, however, needs to be constantly refreshed with a ~60 ns access time. A faster RAM is available in the form of static RAM (SRAM). SRAM allows for much faster access times compared to DRAM (~10 ns) but comprises of six transistors per bit. These more complex structures make SRAM much more expensive and less dense than DRAM and are therefore only commonly found on the level 2 and level 3 cache of a CPU [1]. Unfortunately, SRAM (like DRAM) is volatile memory and is unable to hold its data when power is switched off. Therefore, current research has focussed on developing non-volatile memories that can store information even when the power is switched off. Flash RAM is the most common form of non-volatile RAM. This RAM, while being non-volatile, has issues after 100,000 write cycles leading to deterioration and lowered performance [2].

1.1 Non-Volatile Magnetic RAM (MRAM): Transistor based devices have several drawbacks, one of the largest being the volatility of the stored memory. Power to these devices must be maintained. Once power is lost, the charge of these devices will leak, and the stored data will be erased. One of the current solutions to overcome this issue of volatility, is the use of a magnetic tunnel junction (MTJ). A magnetic tunnel junction is composed of several layers, the three main ones being a hard (fixed) magnetic layer, a thin tunnel barrier, and a soft (free) magnetic layer.

These MTJs store information encoded in the magnetization orientation of the nanomagnetic soft layer, which are able to maintain their state even when power is switched off. However, the many years of head start that the transistor has had over the MTJ has allowed for aggressive optimization of the complementary metal-oxide-semiconductor (CMOS) transistor technology, making it extremely energy efficient compared to switching MTJs with spin polarized current. Hence, current state of the art spin-transfer-torque random access memory (STT-RAM) needs to be switched in a more energy efficient manner.

Current state of the art technology for STT-RAM devices is able to scale down to similar dimensions compared to that of conventional CMOS RAM. However, even when scaled, the energy dissipated by these devices is roughly 1000 times larger than that of the CMOS devices. For example, an experimental demonstration of STT-RAM device scaled to 11 nm lateral dimensions required ~ 100 fJ/bit [3] to switch the magnetization of the soft layer, compared to the ~ 100 aJ/bit energy required to switch CMOS devices [4]. This large energy dissipation leads to very inefficient magnetic memory devices.

1.2 Switching Schemes: MTJ switching, while similar in outcome, function in a variety of ways. Writing data to these MTJs is implemented through the switching of the magnetization of the soft magnetic layer in the MTJ. Most MTJs consist of the same structure between contacts; a fixed magnetic hard layer to polarize the current, a thin tunnel barrier, and a soft magnetic layer (Figure 1.1) that is switched using various methods. Reading of data written to these MTJs is performed by sensing the MTJ resistance. When the two magnetic layers have parallel magnetization orientations, the resistance to the current is low, however when the magnetization orientation of the soft layer is different (antiparallel) to that of the hard layer, there is a much larger resistance.

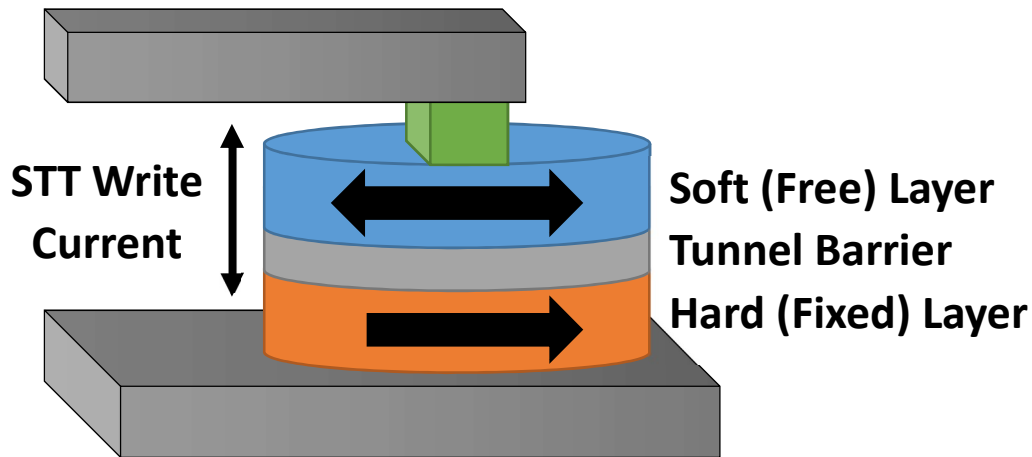


Figure 1.1: General structure of a magnetic tunnel junction.

These differing resistances represent the “1” and “0” bits of the stored data. Switching of the soft magnetic layer is typically achieved using one of these methods: spin-transfer-torque (STT), spin-orbit torque (SOT), voltage controlled magnetic anisotropy (VCMA), use of strain from either applying an electric field to a piezoelectric substrate or strain when surface acoustic waves (SAW) propagate on a piezoelectric substrate.

Spin-transfer-torque (STT) involves applying a current through the hard magnetic layer to polarize electrons that subsequently exert a torque on the magnetization of the soft layer to switch its direction. This differs from a normal read operation as the current for a read operation is much lower than would be needed to switch the magnetization of the soft layer. However, as discussed previously, the energy dissipation to switch STT based MTJ devices is 1000 times higher than that needed to switch current CMOS devices. This could prevent the widespread adoption of pure current driven spin transfer torque (STT) switching that were proposed about 20 years ago [5]–[7].

A newer technology that addresses some of the shortcomings of STT is spin-orbit torque (SOT) induced switching [8]–[10]. However, it results in a 3-terminal memory device that could impede aggressive scaling. Voltage controlled magnetic anisotropy is another mechanism for switching

that utilizes an electric field to switch the nanomagnet instead of current. This rotation can be assisted through coupling with spin-orbit torque or another form of magnetic field. The use of voltage in place of current allows for lower energy dissipation for switching.

Strain generated from a piezoelectric can also be used to alter the magnetization of a nanomagnet of a magnetostrictive material through its magnetomechanical coupling. Figure 1.2 describes the straintronics process in which switching of nanomagnets can be achieved through the use of dipole coupling in conjunction with strain. These schemes, while extremely energy efficient, require complex structures, or must be combined with other methods to achieve switching.

Strain generated via surface acoustic waves (SAW) can also be used to write a bit in an MTJ [11] by controlling the magnetization of its soft magnetostrictive layer. SAW can be created from an

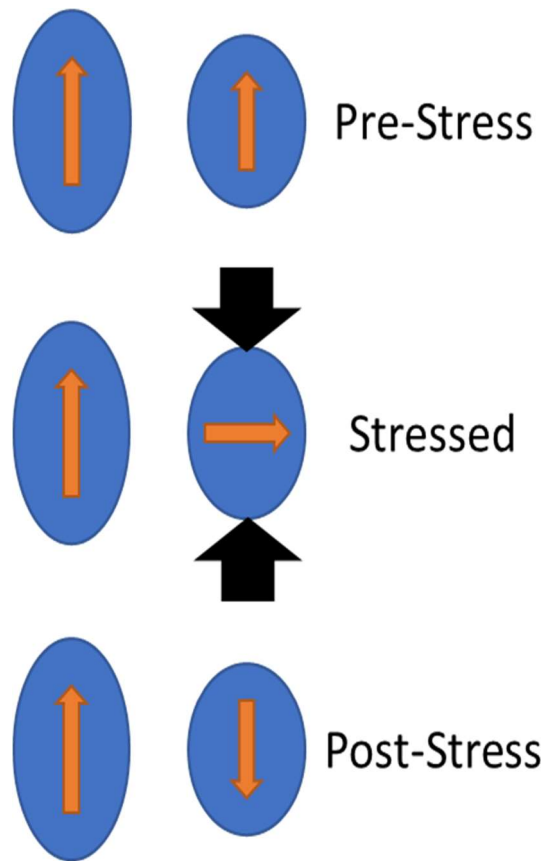


Figure 1.2: Straintronics switching with dipole coupling showing complete reversal of the magnetization.

interdigitated transducer (IDT) fabricated on a piezoelectric substrate which typically produces Rayleigh (transverse) waves. Rotating the magnetization through the use of SAW is very energy efficient, however, only a $\sim 90^\circ$ rotation is possible unless dipole coupling [12] or sequential stress along multiple directions is used [13].

1.3 Scaling Issues with Strain: Mixed mode SAW and STT is a potential alternative to overcoming the large write energy requirement of STT and complexity of SAW devices. Previous efforts have explored this concept in nanomagnets with in-plane magnetization using low frequency SAW [14], which allows for the quasistatic rotation of the magnetization to an approximately known deflection. STT can be applied to achieve switching once this maximum deflection is reached. However, this approach requires a much higher magnitude SAW, especially in scaled nanomagnets as the stress levels required to produce a large deflection of the magnetization increases with decreased volume of the nanomagnets. This is because the uniaxial magnetic anisotropy K_u increases to ensure an energy barrier ~ 1 eV between the “0” and “1” states ($K_u \Omega \approx 1$ eV, where Ω is the volume). Due to this, mixed mode switching has potential issues scaling below 100 nm diameter, with $K_u = (3/2) \cdot \lambda \cdot \sigma$, as the diameter of a circular nanomagnet is decreased by half, the stress (σ) must four times as large to overcome the energy barrier. This issue persists even if moderately magnetostrictive materials such as FeGa [15], [16] are used and even if the Gilbert damping is low. High magnetostrictive materials such as Terfenol-D [17] will not necessarily achieve a larger magnetization deflection with low stress levels due to the bidirectional coupling between magnetization and strain [18]. This further motivates our resonance approach to overcome the limitations associated with quasistatic SAW excitation, allowing for competitive scalability to smaller lateral dimensions.

1.4 Motivation for Combined Resonant SAW and STT: As previously described, scaling to lower dimensions with a combined SAW and STT approach has shown to be impractical due to the increasing stress amplitude needed to affect the magnetization of these nanomagnets in a way as to practically assist the switching process. However, these SAW experiments relied on a low frequency, almost quasistatic, SAW. If the SAW was resonant with the magnetization dynamics of the nanomagnets, it could allow the deflection of the magnetization to build over several cycles, the magnetization could reach a point of deflection that could drastically lower the STT current needed to switch. Figure 1.3 shows the difference between a magnet that was excited by SAW frequencies of both 11 GHz and 11.25 GHz. This small increase in frequency, to the resonant frequency, shows a large increase in deflection, building to almost ($\sim 70^\circ$) completely pointing along the magnetic hard axis. This drastic difference seen from a slight change in the frequency motivates our research into a combined resonant SAW (rSAW) and STT approach to create extremely scalable, low power nanomagnetic switching. While previous work has demonstrated the use of both SAW [19]–[27] and resonant SAW [28], [29] to manipulate the magnetization of nanomagnets (to name a few studies, the list is by no means exhaustive), our study is the first to implement the hybrid approach of using resonant SAW to decrease the write current for STT.

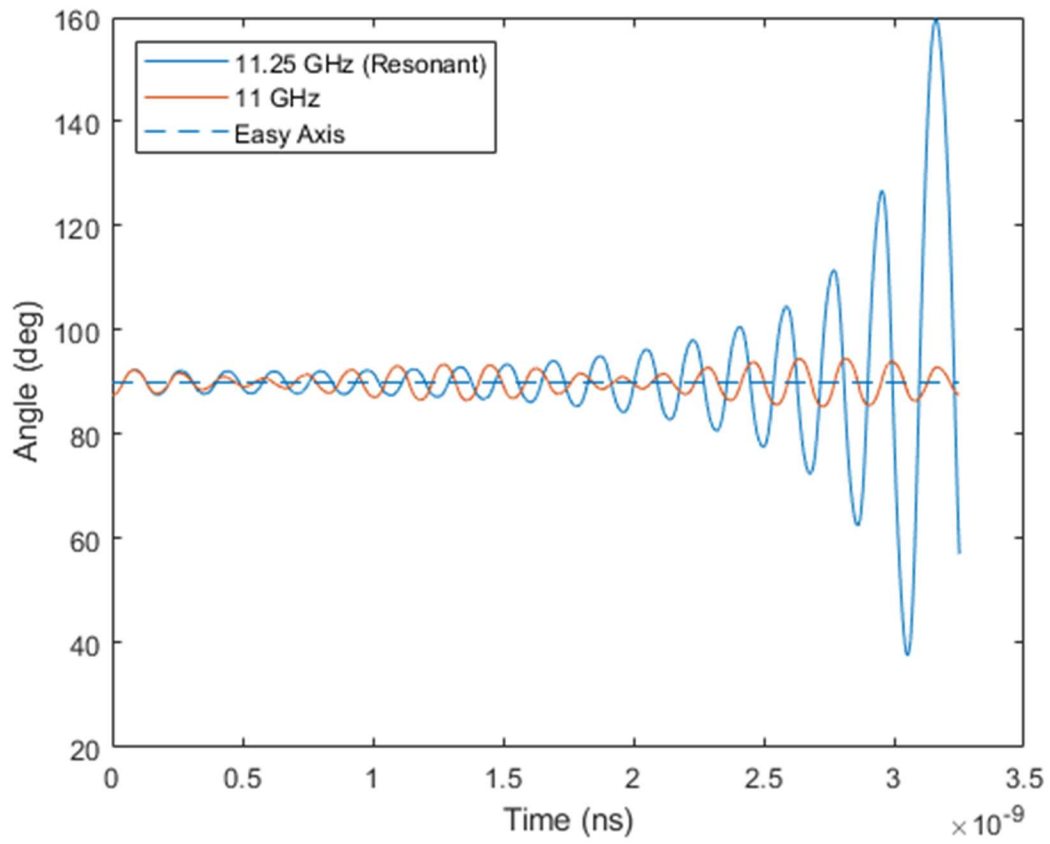


Figure 1.3: Difference in the deflection from the easy axis due to applied SAW of 11 and 11.25 GHz.

Chapter 2: Combined Resonant SAW and STT switching of p-MTJs

To overcome the scalability issues mentioned previously with the mixed mode switching, we study a hybrid resonant SAW and STT scheme to switch the magnetization of nanomagnets for both in-plane and perpendicular-to-plane magnetization. As the magnets are scaled down, more anisotropy is designed into the magnets so as to negate the increasing effects of thermal fluctuations experienced by the magnetization. These anisotropies, determined by shape, volume, interface, and materials, create an energy barrier (E_b) for switching, which we attempt to maintain at $E_b \approx 40$ kT (1 eV). This larger built-in anisotropy requires a larger strain to reduce the switching barrier. Where non-resonant/low frequency excitation of the magnetization effectively applies a quasistatic stress to the magnets. The resonant approach allows the deflection of the magnetization to build over several cycles, ultimately reaching a maximum deflection higher than that of the quasistatic stress of the same magnitude. Figure 2.1 demonstrates how these devices can be realized. The SAW is applied over an entire array of nanomagnets and thus adds very little to the energy

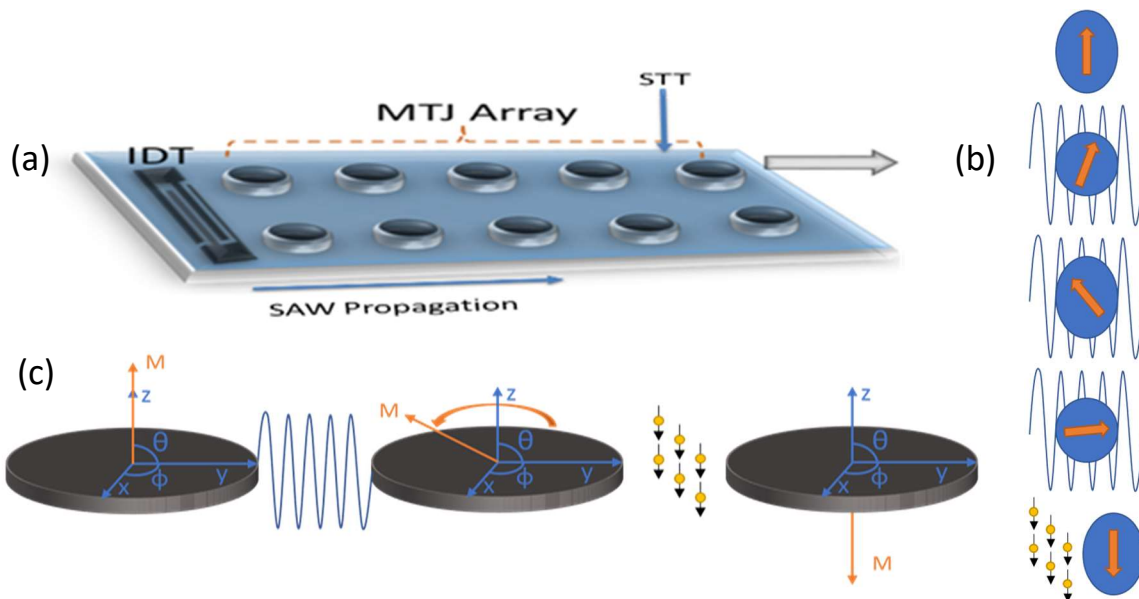


Figure 2.1: (a) MTJ array switched with resonant SAW and STT (b) Magnetization dynamics with resonant SAW + STT switching of in-plane magnetization (c) Magnetization dynamics with resonant SAW + STT switching of out-of-plane magnetization.

dissipation per bit switched. Once the nanomagnets have reached maximum deflection (Figure 2.1(b) for in-plane, and (c) for out-of-plane), spin-transfer-torque can be applied to minimize the spin current required to switch as compared to a non-stressed state.

2.1 Modelling Approach: Modelling of the magnetization dynamics was performed by solving the Landau-Lifshitz-Gilbert (LLG) equation [30] with inclusion of damping like spin transfer torque term [31]:

$$(1 + \alpha^2) \frac{d\vec{M}}{dt} = -\gamma \vec{M} \times \vec{H}_{eff} - \frac{\alpha\gamma}{M_s} [\vec{M} \times (\vec{M} \times \vec{H}_{eff})] + \frac{\alpha\gamma}{M_s} \beta \varepsilon (\vec{M} \times (M_p \times \vec{M})) \quad (1)$$

$$\beta = \left| \frac{\hbar}{\mu_0 e} \right| \frac{J}{l_{th} M_s} \quad (2)$$

where M is the magnetization, γ is the gyromagnetic ratio, α is the Gilbert damping coefficient, M_s is the saturation magnetization and M_p is the magnetization in the direction of the STT polarization, \hbar is the Planck constant, μ_0 is the permeability of free space, e is the charge of an electron, J is the current density of the STT, and l_{th} is the thickness of the nanomagnets. The effective field was calculated from the total energy of the system:

$$\vec{H}_{eff} = -\frac{1}{\mu_0 \Omega} \frac{dE}{d\vec{M}} \quad (3)$$

$$E = E_{stress\ anisotropy} + E_{sha\ anisotropy} + E_{PMA} \quad (4)$$

$$E_{sha\ anisotropy} = \left(\frac{\mu_0}{2} \right) \Omega [N_{d_{xx}} M_x^2 + N_{d_{yy}} M_y^2 + N_{d_{zz}} M_z^2] \quad (5)$$

$$E_{stress\ anisotropy} = -\frac{3}{2} [\lambda_s \sigma \Omega] \sin^2 \theta_i \sin^2 \phi_i \quad (6)$$

$$E_{PMA} = K_{s0} \cos^2 \theta_i \quad (7)$$

with Ω representing the volume of the nanomagnets, N_{d_xx} , N_{d_yy} , and N_{d_zz} the demagnetization factors in the respective directions, λ_s the saturation magnetostriction, σ the stress produced by the SAW on the nanomagnets, θ_i and φ_i the polar and azimuthal angles, respectively, of the magnetization, and K_{s0} the surface anisotropy constant. We note the effective field due to stress is calculated from purely stress (cyclic tension and compression) due to the SAW. The stress in the in-plane direction orthogonal to SAW propagation, which sees the opposite stress (cyclic compression and tension) due to Poisson's effect, is neglected. This does not change the magnetization dynamics qualitatively, and only makes the stress amplitude we estimate conservative (a smaller stress will produce the same effective field if stress in the other direction is accounted for). Table I lists the values of the material properties of $\text{Fe}_{81}\text{Ga}_{19}$ used in these simulations. It was chosen as it has moderate magnetostriction and low Gilbert damping [15], [16].

Table I: FeGa material properties

Parameters	Fe_{0.81}Ga_{0.19}
Saturation Magnetization (M_s)	0.8×10^6 A/m
Gilbert Damping (α)	0.015
Gyromagnetic Ratio (γ)	2.2×10^5
Magnetostriction (λ_s)	350 ppm

The magnetization dynamics were simulated as follows. The resonant SAW was applied for several nanoseconds to build the maximum deflection of the magnetization. The magnitude of the SAW was chosen so that no switching from purely SAW excitation occurs. When the maximum deflection was reached, the minimum STT current density needed to maintain low switching error probability (for example, 99.9% switching in case of out-of-plane switching limited by the number

of computations we could perform) was applied. The time of removal of the SAW (as long as this was after STT application was completed) made no difference to the final switching probability

2.2 In-Plane Switching with SAW and STT: Initial simulation was conducted using elliptical nanomagnetic disks with in-plane magnetic anisotropy as shown in Figure 2.1(b) with dimensions of 40 x 30 nm along the easy and hard axis, respectively, and a thickness of 6 nm. SAW was applied to the nanomagnets and the resonant frequency, which creates the maximum deflection from the magnetic easy axis at the given SAW magnitude, was found. The SAW frequency was found to be double that of the frequency at which the magnetization precesses about the easy axis (Figure 2.2). When the magnet is compressed along its long (easy) axis, the magnetization rotates towards the magnetic hard axis on one side, and when a tensile stress is applied, the magnetization returns to the easy axis. This process is repeated with magnetization moving towards the opposite

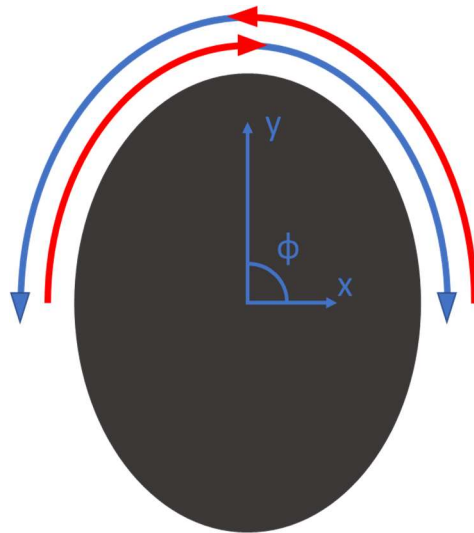


Figure 2.2: Magnetization dynamics of an in-plane nanomagnet with SAW illustrating the doubling of the applied frequency to resonate with one cycle of the motion of the magnetization.

hard axis in the next cycle, leading to a doubling of the frequency for the applied SAW. If resonance is achieved, the deflection of the magnetization from the easy axis will increase until a

maximum deflection is reached over a few 10s of cycles, with frequencies around 10 GHz, this amounts to maximum deflection being reached in as little as a couple of nanoseconds. Without thermal noise (Figure 2.3(a)), the STT current density required (15×10^{11} A/m² with a SAW of 23 MPa at 10.7 GHz) is lowered drastically compared to when no SAW is applied. To achieve switching in the same time without the application of SAW, a current density ~ 3 times larger was needed. This translates to nearly one order of magnitude lower energy (3 times current is 9 times

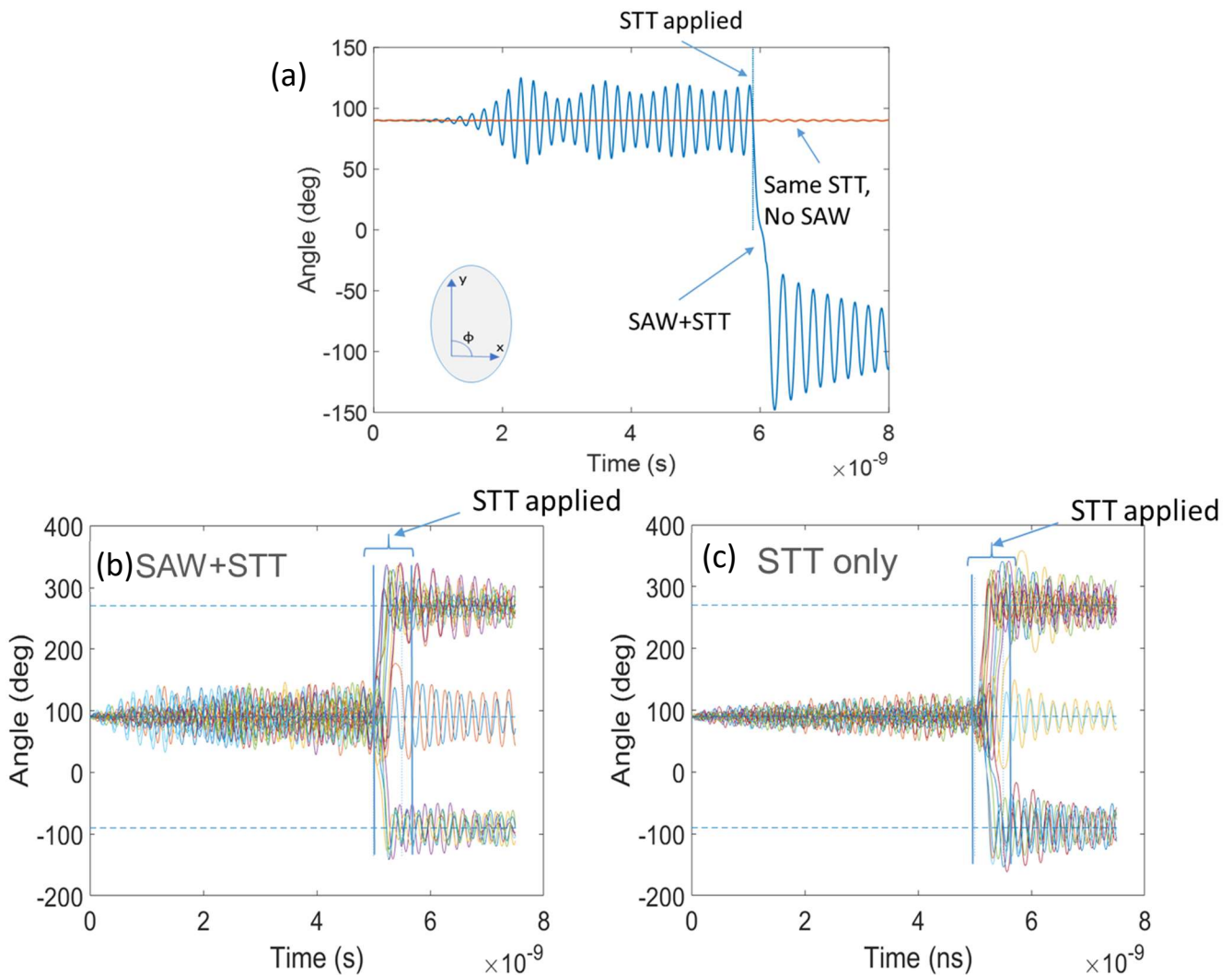


Figure 2.3: In-plane magnetization dynamics simulations with (a) no thermal noise, (b) resonant SAW and STT, and (c) STT only and no SAW. NOTE: Angle shown is the azimuthal angle ϕ with $\sim 90^\circ$ degree being the initial orientation and both $\sim 270^\circ$ and $\sim -90^\circ$ representing a successful switch, while return to $\sim 90^\circ$ degree being an unsuccessful switching event. MATLAB code for (b) and (c) shown in Appendix 1.

write energy, assuming similar application time). However, in the in-plane case, this potential energy saving is severely negated by thermal noise effects as discussed next.

2.3 Thermal Noise: The magnitude of the STT current density needed to achieve 99% switching of the magnetization from the positive to the negative y-axis in the presence of thermal noise and applied SAW of 10 MPa at 9.42 GHz was 10×10^{11} A/m², shown in Figure 2.3(b). Now when the SAW was removed the same current density magnitude sufficed to achieve 99% switching, indicating that the SAW was not helping lower the STT write current for the in-plane switching in the presence of thermal noise (Figure 2.3(c)). This can be explained as follows.

Prior to STT application, a large difference can be seen between the deflection of the magnetization from the thermal noise without SAW to that with thermal noise with SAW. This indicates that the SAW indeed produced higher deflection even with the thermal noise. However, once STT of sufficient magnitude is applied, there is no difference in switching probability between the no-SAW and SAW case. In previous calculations without thermal noise, it was possible to determine a priori the specific timing to apply the STT so that the magnetization is at a point of maximum deflection. However, due to thermal fluctuations, while there is higher deflection with SAW, the inability to apply STT at the maximum deflection (Figure 2.4) negated the benefit of any added deflection from the SAW and no difference was seen between the switching probability in the two cases, as shown in Figure 2.3(b) and 2.3(c).

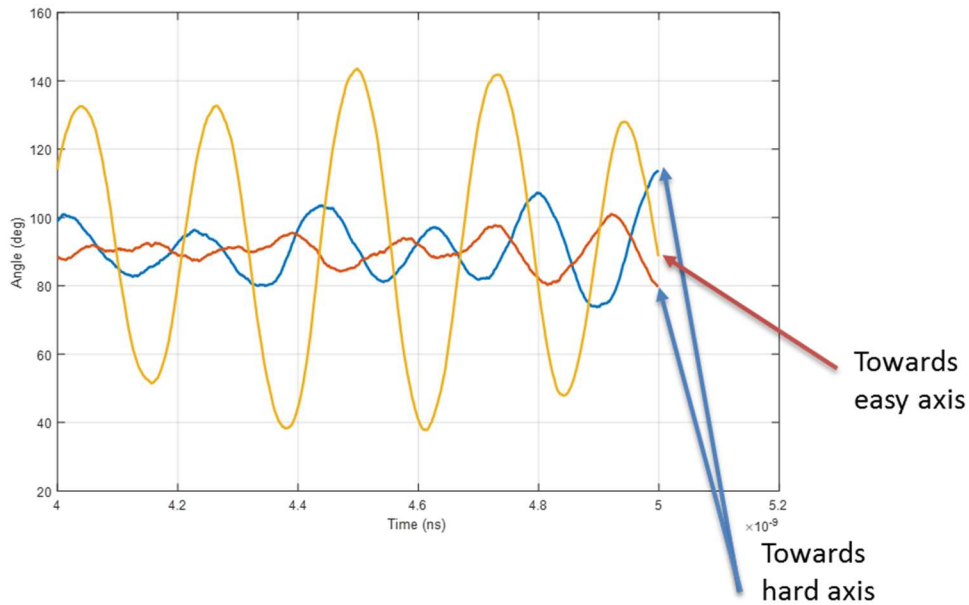


Figure 2.4: Simulation of in-plane magnetization dynamics with thermal effects showing how thermal fluctuations affect timing of the application of the STT.

2.4 Out-of-Plane Switching with SAW and STT: To address the issue of having to time when the STT was applied, as in the in-plane case, magnets with perpendicular magnetic anisotropy were simulated. Simulation of the magnetization dynamics of cylindrical disks with a diameter of 50 nm and thickness 1.5 nm with perpendicular magnetic anisotropy is shown in Figure 2.1 (c). Initially, the magnetization points in the out-of-plane direction (+z-axis), and a continuous SAW was applied across the magnets to find the resonant frequency, which is dependent on the anisotropy of the nanomagnets and magnitude of the SAW (as the oscillation is non-linear). This SAW applies compression and tension along the y-axis of the nanomagnet (and vice versa along the x-axis). This cyclical stressing on the magnet rotates the magnetization from pointing directly out-of-plane to begin to precess about the z-axis, as shown in Figure 2.1(c). As a result of the resonant SAW, the magnetization precesses further from the z-axis and the cone of rotation becomes larger as the magnetization approaches the x-y plane of the nanomagnet.

Once the maximum deflection of the magnetization from the out-of-plane direction was achieved, spin-transfer-torque is applied. As in the previous case, once the magnetization is switched and the STT current is withdrawn, the SAW can be concurrently removed or continued to run for a few cycles before withdrawal as it is not enough to switch the magnetization on its own.

Previously with the in-plane calculations, the inability to selectively apply the STT when the deflection was at a maximum was an issue. However, the manner in which the magnetization precesses around the out-of-plane axis eliminates the need to time the application of the spin torque. This is because for a given polar deflection, θ of the magnetization, which is reached and stabilized after a few cycles, the azimuthal angle, ϕ shown in Figure 2.1 at which the magnetization is oriented when the STT is applied does not affect its efficacy. Once stabilized, the STT is applied to switch the magnetization with regards to θ , therefore, ϕ can be at any point in the precession about the z-axis.

Figure 2.5(a) shows the effect of SAW on deflection of the magnetization with and without thermal fluctuations. Without any SAW, thermal noise alone deflects the magnetization to a maximum of $\sim 10^\circ$ from the z-axis. On the other hand, when SAW of 100 MPa at a resonant frequency of 9.95 GHz is applied and the magnetization allowed to build to its maximum deflection, an average deflection of $\sim 45^\circ$ is seen in both the presence and absence of thermal noise and is achieved in less than 2 nanoseconds. The thermal noise merely makes the deviation from the mean deflection of $\sim 45^\circ$ much higher than the case of precession without thermal noise. Figure 2.5(b) shows the trajectories of magnetization switching in the presence of thermal noise for applied resonant SAW and STT. At a fixed current density and STT application time the switching probabilities (trajectories that switch) are much higher with SAW than without the SAW.

2.5 Out-of-Plane Switching Energy Comparison: At a current density of 1.9×10^{11} A/m² applied for 0.7 ns along with a SAW magnitude of 100 MPa at 9.95 GHz, 99.9% of the simulated nanomagnets successfully switched from the positive to the negative z-axis. Without any SAW, at this same current density and STT application time, roughly 89% of the magnets switched. This error could be reduced to 99.9% in the no SAW case if the current density was doubled to 3.8×10^{11} A/m², as shown in Figure 2.5(c). Simulation of SAW at both 30 MPa at 11.36 GHz and 60 MPa at 10.79 GHz was also conducted and a current density of 3×10^{11} A/m² and 2.2×10^{11} A/m², respectively, was required to achieve 99.9% switching probability. Keeping the current density magnitude fixed at 2×10^{11} A/m² and adjusting the STT application time yielded similar results. While previously, 99.9% of nanomagnets switched at 100 MPa and 0.7 ns, the case with no SAW needed double the amount of time (1.4 ns) to ensure the same switching probability. With required current density being just half that compared to the case without any SAW, the energy savings are four times that of the pure STT case.

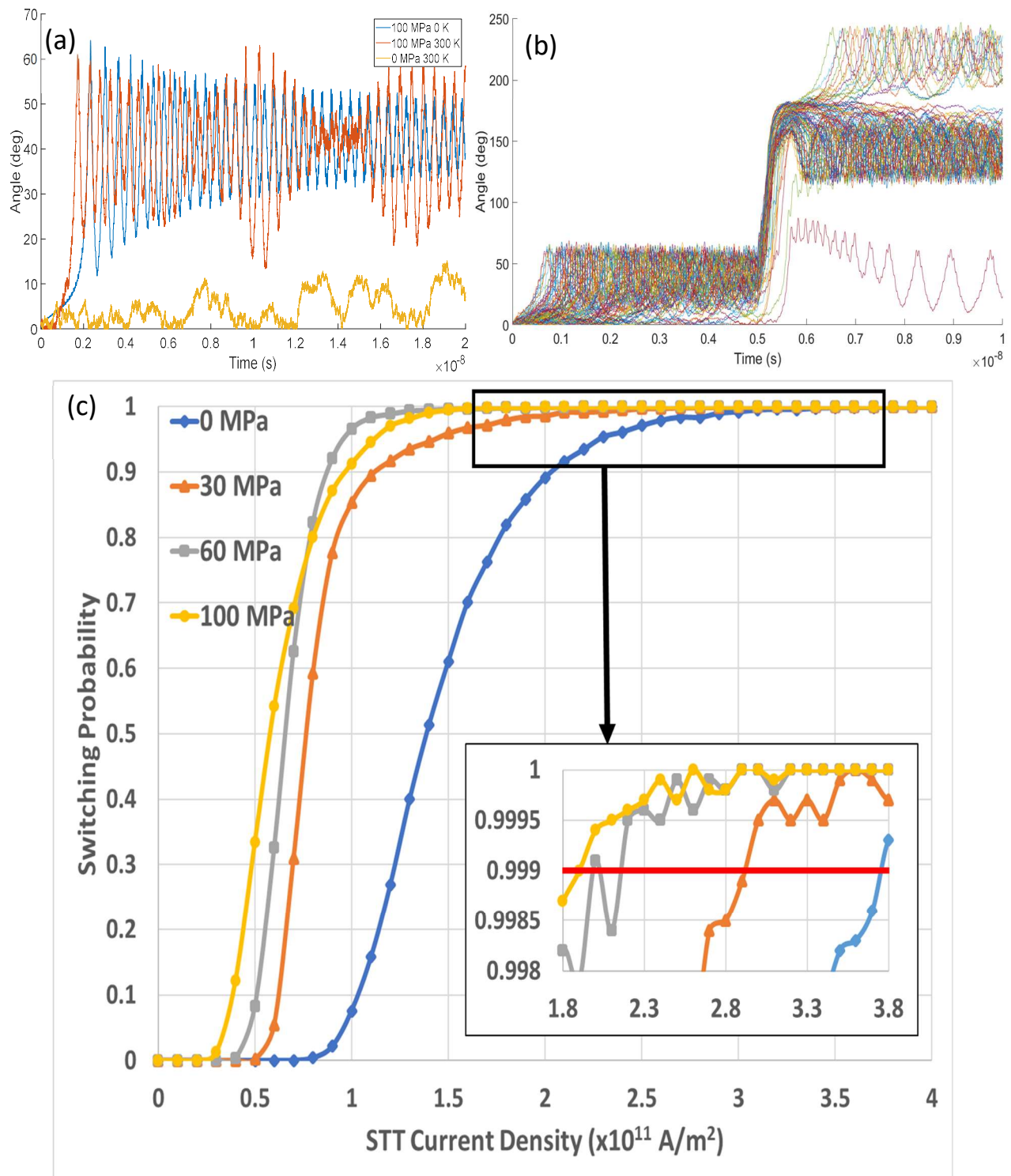


Figure 2.5: Out-of-plane magnetization dynamics simulations with (a) comparison of resonant SAW with and without thermal noise to purely thermal noise and (b) switching of out-of-plane magnetization with resonant SAW and STT (angle shown is the polar angle, θ) (c) Switching probability vs. STT current density of three different SAW magnitudes as well as for no SAW applied. NOTE: MATLAB code for (b) and (c) shown in Appendix 2 and 3.

Chapter 3: Conclusion

In summary, we have shown that application of resonant SAW and STT can be more energy efficient in switching nanomagnetic soft layer of p-MTJs than switching with only STT. This process can be further optimized to increase the energy saving and switching time. These theoretical results could stimulate experimental work, ultimately resulting in the development of more energy efficient STT-RAM.

While we show a four times improvement in energy dissipation, there is potential for at least an order of magnitude reduction in STT write current. One potential approach could use low-moderate magnetostrictive materials with low damping, such as rare earth garnets [32].

Future work could focus on experimental demonstration of this work with perpendicular MTJs, studying if the switching is robust to edge imperfections, material defects, etc. while being scalable. Such investigations of this hybrid approach of using rSAW for STT write current reduction and extreme scalability can lead to MRAM that is competitive with current memory technologies but at the same time non-volatile.

References

- [1] N. Jasuja, “SRAM vs DRAM.” [Online]. Available: https://www.diffen.com/difference/Dynamic_random-access_memory_vs_Static_random-access_memory. [Accessed: 08-Nov-2019].
- [2] “AMD DL160 and DL320 Series Flash: New Densities, New Features,” 22271, 1998. [Online]. Available: http://www.spansion.com/Support/Application_Notes/AMD_DL160_and_DL320_Series_Flash-_New_Densities,_New_Features.pdf. [Accessed: 11-Aug-2019].
- [3] J. J. Nowak *et al.*, “Dependence of Voltage and Size on Write Error Rates in Spin-Transfer Torque Magnetic Random-Access Memory,” *IEEE Magn. Lett.*, vol. 7, pp. 1–4, 2016.
- [4] S. Datta, V. Q. Diep, and B. Behin-Aein, “What constitutes a nanoswitch? A Perspective,” Apr. 2014.
- [5] J. C. Slonczewski, “Current-driven excitation of magnetic multilayers,” *J. Magn. Magn. Mater.*, vol. 159, no. 1–2, pp. L1–L7, Jun. 1996.
- [6] L. Berger, “Emission of spin waves by a magnetic multilayer traversed by a current,” *Phys. Rev. B*, vol. 54, no. 13, pp. 9353–9358, Oct. 1996.
- [7] D. C. Ralph and M. D. Stiles, “Spin transfer torques,” *J. Magn. Magn. Mater.*, vol. 320, no. 7, pp. 1190–1216, Apr. 2008.
- [8] L. Liu, C.-F. Pai, Y. Li, H. W. Tseng, D. C. Ralph, and R. A. Buhrman, “Spin-torque switching with the giant spin Hall effect of tantalum,” *Science*, vol. 336, no. 6081, pp. 555–8, May 2012.

- [9] D. Bhowmik, L. You, and S. Salahuddin, “Spin Hall effect clocking of nanomagnetic logic without a magnetic field,” *Nat. Nanotechnol.*, vol. 9, no. 1, pp. 59–63, Jan. 2014.
- [10] I. Mihai Miron *et al.*, “Current-driven spin torque induced by the Rashba effect in a ferromagnetic metal layer,” *Nat. Mater.*, vol. 9, no. 3, pp. 230–234, Mar. 2010.
- [11] N. D’Souza *et al.*, “Energy-efficient switching of nanomagnets for computing: Straintronics and other methodologies,” *Nanotechnology*, vol. 29, no. 44, p. 49, 2018.
- [12] V. Sampath, N. D’Souza, G. M. Atkinson, S. Bandyopadhyay, and J. Atulasimha, “Experimental demonstration of acoustic wave induced magnetization switching in dipole coupled magnetostrictive nanomagnets for ultralow power computing,” *Appl. Phys. Lett.*, vol. 109, no. 10, p. 102403, Sep. 2016.
- [13] A. K. Biswas, H. Ahmad, J. Atulasimha, and S. Bandyopadhyay, “Experimental Demonstration of Complete 180° Reversal of Magnetization in Isolated Co Nanomagnets on a PMN–PT Substrate with Voltage Generated Strain,” *Nano Lett.*, vol. 17, no. 6, pp. 3478–3484, Jun. 2017.
- [14] A. K. Biswas, S. Bandyopadhyay, and J. Atulasimha, “Acoustically assisted spin-transfer-torque switching of nanomagnets: An energy-efficient hybrid writing scheme for non-volatile memory,” *Appl. Phys. Lett.*, vol. 103, no. 23, p. 232401, Dec. 2013.
- [15] A. Clark, M. Wun-Fogle, J. B. Restorff, and T. A. Lograsso, “Magnetostrictive Properties of Galfenol Alloys Under Compressive Stress,” *Mater. Trans.*, vol. 43, no. 5, pp. 881–886, 2002.
- [16] D. B. Gopman, V. Sampath, H. Ahmad, S. Bandyopadhyay, and J. Atulasimha, “Static

- and Dynamic Magnetic Properties of Sputtered Fe-Ga Thin Films,” *IEEE Trans. Magn.*, vol. 53, no. 11, Nov. 2017.
- [17] L. Sandlund, M. Fahlander, T. Cedell, A. E. Clark, J. B. Restorff, and M. Wun-Fogle, “Magnetostriction, elastic moduli, and coupling factors of composite Terfenol-D,” *J. Appl. Phys.*, vol. 75, no. 10, pp. 5656–5658, May 1994.
- [18] Z. Xiao *et al.*, “Bi-directional coupling in strain-mediated multiferroic heterostructures with magnetic domains and domain wall motion.”
- [19] L. Thevenard *et al.*, “Precessional magnetization switching by a surface acoustic wave,” *Phys. Rev. B*, vol. 93, p. 134430, 2016.
- [20] L. Thevenard *et al.*, “Surface-acoustic-wave-driven ferromagnetic resonance in (Ga,Mn)(As,P) epilayers,” *Phys. Rev. B*, vol. 90, p. 94401, 2014.
- [21] M. Weiler *et al.*, “Elastically Driven Ferromagnetic Resonance in Nickel Thin Films,” 2011.
- [22] L. Thevenard *et al.*, “Strong reduction of the coercivity by a surface acoustic wave in an out-of-plane magnetized epilayer,” *RAPID Commun. Phys. Rev. B*, vol. 93, p. 140405, 2016.
- [23] W. Li, B. Buford, A. Jander, and P. Dhagat, “Magnetic recording with acoustic waves,” *Phys. B Condens. Matter*, vol. 448, pp. 151–154, Sep. 2014.
- [24] W. Li, B. Buford, A. Jander, and P. Dhagat, “Acoustically Assisted Magnetic Recording: A New Paradigm in Magnetic Data Storage,” *IEEE Trans. Magn.*, vol. 50, no. 3, pp. 37–40, Mar. 2014.

- [25] W. Li, B. Buford, A. Jander, and P. Dhagat, “Writing magnetic patterns with surface acoustic waves,” *J. Appl. Phys.*, vol. 115, pp. 17–307, 2014.
- [26] L. Thevenard *et al.*, “Irreversible magnetization switching using surface acoustic waves,” *Phys. Rev. B*, vol. 87, p. 144402, 2013.
- [27] S. Davis, A. Baruth, and S. Adenwalla, “Magnetization dynamics triggered by surface acoustic waves,” *Appl. Phys. Lett.*, vol. 97, no. 23, p. 232507, Dec. 2010.
- [28] D. Labanowski *et al.*, “Voltage-driven, local, and efficient excitation of nitrogen-vacancy centers in diamond,” *Sci. Adv.*, vol. 4, no. 9, p. eaat6574, Sep. 2018.
- [29] J. Janušonis, C. L. Chang, P. H. M. van Loosdrecht, and R. I. Tobey, “Frequency tunable surface magneto elastic waves,” *Appl. Phys. Lett.*, vol. 106, no. 18, p. 181601, May 2015.
- [30] T. L. Gilbert, “Classics in Magnetism A Phenomenological Theory of Damping in Ferromagnetic Materials,” *IEEE Trans. Magn.*, vol. 40, no. 6, pp. 3443–3449, Nov. 2004.
- [31] J. Z. Sun, “Spin-current interaction with a monodomain magnetic body: A model study,” *Phys. Rev. B*, vol. 62, no. 1, pp. 570–578, Jul. 2000.
- [32] E. R. Rosenberg *et al.*, “Magnetism and spin transport in rare-earth-rich epitaxial terbium and europium iron garnet films,” *Phys. Rev. Mater.*, vol. 2, p. 94405, 2018.

APPENDIX

1. MATLAB code for 2.3(b) and 2.3(c)

```
clc, clear all, close all
tic
%%%%%%%%%%%%%%%%%%%%%%%%%%%%%%%%%%%%%%%%%%%%%%%%%%%%%%%%%%%%%%%%%%%%%%%%
%CONSTRAINTS
T = 300; % [K] Temperature
sig = 10e6; % [MPa] Stress applied in the Y-direction, (-)
           %=compression
frequency = 4.71e9*2; % [Hz] Stress Frequency
sttstart = 5e3; % [ps] Time When STT is Started
stttime = 0.5e3; % [ps] How Long STT is Applied
sttbuidup = 0e3;
sttrampdown = 0.5e3;
rest = 2e3; % [ps] Time at End to Allow Magnets to Rest
tf = (sttstart+stttime+rest)*10^-12; % [s] Run Length
stresstime = sttstart+0.3e3; % [ps] Applied Stress Time
J = -10e11;
P = 0.8;
dif = 6; % Number of peaks to skip when finding average
m = 20; % Number of simulations to run
bias = 0; % Set to 1 for Bias Magnet
%thermal = 0; % Set to 1 for thermal noise
freqfind = 1; % Set to 1 to find resonant frequency
%%%%%%%%%%%%%%%%%%%%%%%%%%%%%%%%%%%%%%%%%%%%%%%%%%%%%%%%%%%%%%%%%%%%%%%%
% Constants
mu_0 = 4*pi*10^(-7); % [H/m] Permeability of Free Space
K = 1.3806e-23; % [m^2*kg/(s^2*K)] Boltzmann Constant
h_bar = (6.634e-34)/(2*pi);
e = 1.6e-19;
% Parameters
a = 40e-9; % [m] Major Axis Diameter
b = 30e-9; % [m] Minor Axis Diameter
th = 6e-9; % [m] Thickness
Omega = 0.25*pi*a*b*th; % [m^3] Volume
a1 = 102.75e-9; % [m] Major Axis Diameter
b1 = 98.25e-9; % [m] Minor Axis Diameter
th1 = 10e-9; % [m] Thickness
Omega1 = 0.25*pi*a1*b1*th1; % [m^3] Volume
M_s = 0.8e6; % [A/m] Saturation Magnetization
alpha = 0.015; % [-] Gilbert Damping Constant
gamma = 2.2e5; % [-] Gyromagnetic Ratio
lambda_s = 300e-6; % [-] Magnetostriction
R = 200e-9; % [m] Center Distance Between Magnets
% Time
```

```

dt = 1e-12;                %[s] Time Step
n = int16((tf/dt)+1);     %Number of Steps
t = 0:dt:tf+dt;
freq = zeros(m,1);
freq(1) = frequency;
K_eff = 40*(K*T)/(Omega)
K_s0 = (K_eff+mu_0*M_s^2/2)
phimax = zeros(m,1);
phimin = zeros(m,1);
% Shape Anisotropy
N_d_yy = (pi/4)*(th/a)*(1-(1/4)*((a-b)/a)-(3/16)*((a-b)/a)^2);
N_d_xx = (pi/4)*(th/a)*(1+(5/4)*((a-b)/a)+(21/16)*((a-b)/a)^2);
N_d_zz = 1-(pi/4)*(th/a)*(2+((a-b)/a)+(18/16)*((a-b)/a)^2);
N_d_yy1 = (pi/4)*(th1/a1)*(1-(1/4)*((a1-b1)/a1)-(3/16)*((a1-b1)/a1)^2);
N_d_xx1 = (pi/4)*(th1/a1)*(1+(5/4)*((a1-b1)/a1)+(21/16)*((a1-b1)/a1)^2);
N_d_zz1 = 1-(pi/4)*(th1/a1)*(2+((a1-b1)/a1)+(18/16)*((a1-b1)/a1)^2);
Check = N_d_xx+N_d_yy+N_d_zz;    %Check Should = 1
switching = zeros(m,1);
success = zeros(m,1);
barrier = mu_0*M_s^2*(N_d_xx-N_d_yy)/(3*lambda_s);
theta = zeros(n,1);
phi = zeros(n,1);
theta1 = zeros(n,1);
phi1 = zeros(n,1);
m_x = zeros(n,1);
m_y = zeros(n,1);
m_z = zeros(n,1);
m_x1 = zeros(n,1);
m_y1 = zeros(n,1);
m_z1 = zeros(n,1);
var = 2*alpha*K*T/(dt*gamma*M_s*Omega*mu_0);
var1 = 2*alpha*K*T/(dt*gamma*M_s*Omega1*mu_0);
epsilon = P/2;
beta = zeros(n+1,1);
sigma = zeros(n,1);
for j = 1:m

    %Initial Conditions
    theta(1) = 89.9*pi/180;    %[rad] Polar Magnetization Angle
    phi(1) = 89.84*pi/180;    %[rad] Azimuthal Magnetization Angle

    theta1(1) = 89.9*pi/180;  %[rad] Polar Magnetization Angle of Bias Magnet
    phi1(1) = 89.9*pi/180;   %[rad] Azimuthal Magnetization Angle of Bias
Magnet

    m_y(1) = sin(theta(1))*sin(phi(1));
    m_x(1) = sin(theta(1))*cos(phi(1));
    m_z(1) = cos(theta(1));

    m_y1(1) = sin(theta1(1))*sin(phi1(1));

```



```

m_x1(1) = sin(theta1(1))*cos(phi1(1));
m_z1(1) = cos(theta1(1));

thermal_x = sqrt(var)*randn(1,n);
thermal_y = sqrt(var)*randn(1,n);
thermal_z = sqrt(var)*randn(1,n);
thermal_x1 = sqrt(var1)*randn(1,n);
thermal_y1 = sqrt(var1)*randn(1,n);
thermal_z1 = sqrt(var1)*randn(1,n);

for i = 1:n
    counting = zeros(n+1,1);
    counting(i) = i;

    if i <= stresstime
        if T > 0
            sigma(i) = -sig*cos(2*pi*t(i)*freq(1));
        else
            sigma(i) = -sig*cos(2*pi*t(i)*freq(j));
        end

        H_eff_x = bias*(M_s*Omega/(4*pi*R^3))*(2*sin(theta1(i))*...
            cos(phi1(i)))-
M_s*N_d_xx*sin(theta(i))*cos(phi(i))+thermal_x(1,i);
        H_eff_y = -bias*(M_s*Omega/(4*pi*R^3))*(sin(theta1(i))*...
            sin(phi1(i)))-M_s*N_d_yy*sin(theta(i))*sin(phi(i))+...
(3*lambda_s/(mu_0*M_s))*sigma(i)*sin(theta(i))*sin(phi(i))+thermal_y(1,i);
        H_eff_z = -bias*(M_s*Omega/(4*pi*R^3))*(cos(theta1(i)))-...
            M_s*N_d_zz*cos(theta(i))+thermal_z(1,i);

        else
            sigma(i) = 0;                %Stress applied in the Y-direction, (-
)=compression

            H_eff_x = bias*(M_s*Omega/(4*pi*R^3))*(2*sin(theta1(i))*...
                cos(phi1(i)))-
M_s*N_d_xx*sin(theta(i))*cos(phi(i))+thermal_x(1,i);
            H_eff_y = -bias*(M_s*Omega/(4*pi*R^3))*(sin(theta1(i))*...
                sin(phi1(i)))-M_s*N_d_yy*sin(theta(i))*sin(phi(i))+...
(3*lambda_s/(mu_0*M_s))*sigma(i)*sin(theta(i))*sin(phi(i))+thermal_y(1,i);
            H_eff_z = -bias*(M_s*Omega/(4*pi*R^3))*(cos(theta1(i)))-...
                M_s*N_d_zz*cos(theta(i))+thermal_z(1,i);

        end

        if i <= sttstart || i > (stttime+sttstart)
            beta(i) = 0;
        elseif i > sttstart && i <= (sttstart+sttbuildup)
            slope = (h_bar*J/(th*M_s*mu_0*e))/(sttbuildup);

```

```

        beta(i) = slope*(counting(i)-sttstart);
elseif i > (sttstart+(stttime-sttrampdown)) && i <= (sttstart+stttime)
    slope = (h_bar*J/(th*M_s*mu_0*e))/(sttrampdown);
    beta(i) = -slope*(counting(i)-(sttstart+stttime));
else
    beta(i) = h_bar*J/(th*M_s*mu_0*e);
end

m_x(i) = -gamma*(H_eff_z*sin(theta(i))*sin(phi(i))...
-H_eff_y*cos(theta(i)))...
-
alpha*gamma*(H_eff_y*sin(theta(i))*cos(phi(i))*sin(theta(i))*sin(phi(i))...
-H_eff_x*(sin(theta(i))*sin(phi(i)))*(sin(theta(i))*sin(phi(i)))...
-H_eff_x*cos(theta(i))*cos(theta(i))...
+H_eff_z*sin(theta(i))*cos(phi(i))*cos(theta(i)))...
+gamma*beta(i)*epsilon*(sin(theta(i))*sin(phi(i)))*(sin(theta(i))*cos(phi(i)));

m_y(i) = -gamma*(H_eff_x*cos(theta(i))...
-H_eff_z*sin(theta(i))*cos(phi(i)))...
-alpha*gamma*(H_eff_z*sin(theta(i))*sin(phi(i))*cos(theta(i))...
-H_eff_y*cos(theta(i))*cos(theta(i))...
-H_eff_y*(sin(theta(i))*cos(phi(i)))*(sin(theta(i))*cos(phi(i)))...
+H_eff_x*sin(theta(i))*cos(phi(i))*sin(theta(i))*sin(phi(i)))...
+gamma*beta(i)*epsilon*(sin(theta(i))*cos(phi(i))*sin(theta(i))*cos(phi(i))+cos(t
heta(i))*cos(theta(i)));

m_z(i) = sqrt(1-(m_y(i)^2+m_x(i)^2));
theta(i+1) =
theta(i)+dt*(m_x(i)*cos(phi(i))+m_y(i)*sin(phi(i)))/cos(theta(i));
phi(i+1) = phi(i)+dt*(m_y(i)*cos(phi(i))-
m_x(i)*sin(phi(i)))/sin(theta(i));

%%%%%%%%%%%%%%%%%%%%%%%%%%%%%%%%%%%%%%%%%%%%%%%%%%%%%%%%%%%%%%%%%%%%%%%%
% Ignore this if no bias magnet
if i <= stresstime %Bias Magnet Loop
    %sigma(i) = -5e6*sin(t(i))*1e9);
    H_eff_x1 = bias*(M_s*Omega1/(4*pi*R^3))*(2*sin(theta(i))*...
        cos(phi(i)))-
M_s*N_d_xx1*sin(theta1(i))*cos(phi1(i))+thermal_x1(1,i);
    H_eff_y1 = -bias*(M_s*Omega1/(4*pi*R^3))*(sin(theta(i))*...
        sin(phi(i)))-M_s*N_d_yy1*sin(theta1(i))*sin(phi1(i))+...
(3*lambda_s/(mu_0*M_s))*sigma(i)*sin(theta1(i))*sin(phi1(i))+thermal_y1(1,i);
    H_eff_z1 = -bias*(M_s*Omega1/(4*pi*R^3))*(cos(theta(i)))-...
        M_s*N_d_zz1*cos(theta1(i))+thermal_z1(1,i);

else
    sigma(i) = 0;

```

```

        H_eff_x1 = bias*(M_s*Omega1/(4*pi*R^3))*(2*sin(theta(i))*...
            cos(phi(i)))-
M_s*N_d_xx1*sin(theta1(i))*cos(phi1(i))+thermal_x1(1,i);
        H_eff_y1 = -bias*(M_s*Omega1/(4*pi*R^3))*(sin(theta(i))*...
            sin(phi(i)))-M_s*N_d_yy1*sin(theta1(i))*sin(phi1(i))+...
(3*lambda_s/(mu_0*M_s))*sigma(i)*sin(theta1(i))*sin(phi1(i))+thermal_y1(1,i);
        H_eff_z1 = -bias*(M_s*Omega1/(4*pi*R^3))*(cos(theta(i)))-...
            M_s*N_d_zz1*cos(theta1(i))+thermal_z1(1,i);
    end

    m_x1(i) = gamma*(H_eff_z1*sin(theta1(i))*sin(phi1(i))...
        -H_eff_y1*cos(theta1(i)))...
-
alpha*gamma*(H_eff_y1*sin(theta1(i))*cos(phi1(i))*sin(theta1(i))*sin(phi1(i))...
    -H_eff_x1*(sin(theta1(i))*sin(phi1(i)))^2)...
    -H_eff_x1*cos(theta1(i))^2)...
    +H_eff_z1*sin(theta1(i))*cos(phi1(i))*cos(theta1(i)));

    m_y1(i) = gamma*(H_eff_x1*cos(theta1(i))...
        -H_eff_z1*sin(theta1(i))*cos(phi1(i)))...
    -alpha*gamma*(H_eff_z1*sin(theta1(i))*sin(phi1(i))*cos(theta1(i))...
    -H_eff_y1*cos(theta1(i))^2)...
    -H_eff_y1*(sin(theta1(i))*cos(phi1(i)))^2)...
    +H_eff_x1*sin(theta1(i))*cos(phi1(i))*sin(theta1(i))*sin(phi1(i)));

    m_z1(i) = sqrt(1-(m_y1(i)^2+m_x1(i)^2));
%%%%%%%%%%%%%%%%%%%%%%%%%%%%%%%%%%%%%%%%%%%%%%%%%%%%%%%%%%%
    theta1(i+1) =
theta1(i)+dt*((m_x1(i)*cos(phi1(i))+m_y1(i)*sin(phi1(i)))/cos(theta1(i)));
    phi1(i+1) = phi1(i)+dt*((m_y1(i)*cos(phi1(i))-
m_x1(i)*sin(phi1(i)))/sin(theta1(i)));
    end

    sigma(i+1) = 0;
    phi = phi*180/pi;
    phi1 = phi1*180/pi;

    if bias == 1
        plot (t,phi,t,phi1)
    else
        plot (t,phi)
        hold on;
    end

    end

    line([0,tf],[ -90,-90], 'linestyle', '--')

```

```

line([0,tf],[270,270], 'linestyle', '--')
line([(sttstart)*10^-12,(sttstart)*10^-12],[-135,315], 'linestyle', ':')
line([(sttstart+stttime)*10^-12,(sttstart+stttime)*10^-12],[-
135,315], 'linestyle', ':')
[pks,locs,w,p] = findpeaks(phi);
format long

if freqfind == 1
    period1 = locs(2+dif)-locs(1+dif);
    period2 = locs(3+dif)-locs(2+dif);
    period3 = locs(4+dif)-locs(3+dif);
    period4 = locs(5+dif)-locs(4+dif);
    period5 = locs(6+dif)-locs(5+dif);
    freq(j+1) = 2*1e12/((period1+period2+period3+period4)/4);
end

phimax(j,1) = max(phi(1:sttstart));
phimin(j,1) = min(phi(1:sttstart));

if max(phi) > 180 || min(phi) < 0
    switching(j) = 1;

else
    switching(j) = 0;

end

if 230 <= phi(end) && phi(end) <= 310
    success(j) = 1;

elseif -130 <= phi(end) && phi(end) <= -50
    success(j) = 1;

else
    success(j) = 0;

end

end

line([0,tf],[90,90], 'linestyle', '--')
xlabel('Time (ns)')
ylabel('Angle (deg)')
maxphi = max(phimax);
minphi = min(phimin);
avg_phimax = sum(phimax(:,1))/m
avg_phimin = sum(phimin(:,1))/m
Frequencies = freq(1:j)/2;
switching_chance = sum(switching)/m
success_chance = sum(success)/m
figure(2)

```

```

plot (t,sigma)
figure(3)
plot (t,beta(1:i+1))
toc

```

2. MATLAB code for 2.5(b)

```

clc, clearvars, close all
tic
%%%%%%%%%%%%%%%%%%%%%%%%%%%%%%%%%%%%%%%%%%%%%%%%%%%%%%%%%%%%%%%%%%%%%%%%
%CONSTRAINTS
T = 300;           %[K] Temperature
sig = 100e6;      %[MPa] Stress applied in the Y-direction, (-
)=compression
frequency = 9.95e9;  %[Hz] Stress Frequency
freqdiff = 0.0e9;
sttstart = 5e3;     %[ps] Time When STT is Started
stttime = 0.7e3;   %[ps] How Long STT is Applied
sttbuildup = 0e3;
sttrampdown = 0e3;
sttfield = 0e3;
rest = 5e3;        %[ps] Time at End to Allow Magnets to Rest
tf = (sttstart+stttime+rest)*10^-12;  %[s] Run Length
stresstime = tf*10^12;  %[ps] Applied Stress Time
J = 1.9e11;
Jlow = 0*-1.5e11;
P = 0.8;
dif = 6;           %Number of peaks to skip when finding average
m = 100;           %Number of simulations to run
bias = 0;          %Set to 1 for Bias Magnet
%thermal = 0;     %Set to 1 for thermal noise
freqfind = 0;     %Set to 1 to find resonant frequency
%%%%%%%%%%%%%%%%%%%%%%%%%%%%%%%%%%%%%%%%%%%%%%%%%%%%%%%%%%%%%%%%%%%%%%%%
% Constants
mu_0 = 4*pi*10^(-7);  %[H/m] Permeability of Free Space
K = 1.3806e-23;      %[m^2*kg/(s^2*K)] Boltzmann Constant
h_bar = (6.634e-34)/(2*pi);
e = 1.6e-19;
% Parameters
a = 50e-9;          %[m] Major Axis Diameter
b = 50e-9;          %[m] Minor Axis Diameter
th = 1.5e-9;        %[m] Thickness
Omega = 0.25*pi*a*b*th;  %[m^3] Volume
a1 = 102.75e-9;     %[m] Major Axis Diameter
b1 = 98.25e-9;      %[m] Minor Axis Diameter
th1 = 10e-9;        %[m] Thickness

```

```

Omega1 = 0.25*pi*a1*b1*th1;      %[m^3] Volume
M_s = 0.8e6;                    %[A/m] Saturation Magnetization
alpha = 0.015;                 %[-] Gilbert Damping Constant
gamma = 2.2e5;                 %[-] Gyromagnetic Ratio
lambda_s = 350e-6;            %[-] Magnetostriction
R = 200e-9;                   %[m] Center Distance Between Magnets
% Time
dt = 1e-12;                   %[s] Time Step
n = int16((tf/dt)+1);         %Number of Steps
t = 0:dt:tf+dt;
freq = zeros(m,1);
freq(1) = frequency;
K_eff = 40*(K*300)/(Omega)
K_s0 = (K_eff+mu_0*M_s^2/2)*th
phimax = zeros(m,1);
phimin = zeros(m,1);
% Shape Anisotropy
N_d_yy = (pi/4)*(th/a)*(1-(1/4)*((a-b)/a)-(3/16)*((a-b)/a)^2);
N_d_xx = (pi/4)*(th/a)*(1+(5/4)*((a-b)/a)+(21/16)*((a-b)/a)^2);
N_d_zz = 1-(pi/4)*(th/a)*(2+((a-b)/a)+(18/16)*((a-b)/a)^2);
N_d_yy1 = (pi/4)*(th1/a1)*(1-(1/4)*((a1-b1)/a1)-(3/16)*((a1-b1)/a1)^2);
N_d_xx1 = (pi/4)*(th1/a1)*(1+(5/4)*((a1-b1)/a1)+(21/16)*((a1-b1)/a1)^2);
N_d_zz1 = 1-(pi/4)*(th1/a1)*(2+((a1-b1)/a1)+(18/16)*((a1-b1)/a1)^2);
Check = N_d_xx+N_d_yy+N_d_zz;   %Check Should = 1
switching = zeros(m,1);
success = zeros(m,1);
barrier = mu_0*M_s^2*(N_d_xx-N_d_yy)/(3*lambda_s)
theta = zeros(n,1);
phi = zeros(n,1);
theta1 = zeros(n,1);
phi1 = zeros(n,1);
m_x = zeros(n,1);
m_y = zeros(n,1);
m_z = zeros(n,1);
m_x1 = zeros(n,1);
m_y1 = zeros(n,1);
m_z1 = zeros(n,1);
var = 2*alpha*K*T/(dt*gamma*M_s*Omega*mu_0);
var1 = 2*alpha*K*T/(dt*gamma*M_s*Omega1*mu_0);
epsilon = P/2;
beta = zeros(n+1,1);
sigma = zeros(n,1);
thetamax = zeros(m,1);
thetamin = zeros(m,1);
avg_final = zeros(m,1);
for j = 1:m

    %Initial Conditions
    theta(1) = 1*pi/180;        %[rad] (90 is in plane) Polar Magnetization Angle
    phi(1) = 89.84*pi/180;     %[rad] Azimuthal Magnetization Angle

```

```

theta1(1) = 89.9*pi/180;    %[rad] (90 is in plane) Polar Magnetization Angle
of Bias Magnet
phi1(1) = 89.9*pi/180;    %[rad] Azimuthal Magnetization Angle of Bias
Magnet

m_y(1) = sin(theta(1))*sin(phi(1));
m_x(1) = sin(theta(1))*cos(phi(1));
m_z(1) = cos(theta(1));

m_y1(1) = sin(theta1(1))*sin(phi1(1));
m_x1(1) = sin(theta1(1))*cos(phi1(1));
m_z1(1) = cos(theta1(1));

thermal_x = sqrt(var)*randn(1,n);
thermal_y = sqrt(var)*randn(1,n);
thermal_z = sqrt(var)*randn(1,n);
thermal_x1 = sqrt(var1)*randn(1,n);
thermal_y1 = sqrt(var1)*randn(1,n);
thermal_z1 = sqrt(var1)*randn(1,n);

for i = 1:n
    counting = zeros(n+1,1);
    counting(i) = i;

    if i <= stresstime
        if T > 0
            sigma(i) = -sig*sin(2*pi*t(i)*freq(j));

        else
            sigma(i) = -sig*sin(2*pi*t(i)*freq(j));
        end

        H_eff_x = -M_s*N_d_xx*sin(theta(i))*cos(phi(i))+thermal_x(1,i);
        H_eff_y = -M_s*N_d_yy*sin(theta(i))*sin(phi(i))+...
(3*lambda_s/(mu_0*M_s))*sigma(i)*sin(theta(i))*sin(phi(i))+thermal_y(1,i);
        H_eff_z = -
M_s*N_d_zz*cos(theta(i))+thermal_z(1,i)+2*K_s0*cos(theta(i))/(mu_0*M_s*th);

        else
            sigma(i) = 0;                %Stress applied in the Y-direction, (-
)=compression

            H_eff_x = -M_s*N_d_xx*sin(theta(i))*cos(phi(i))+thermal_x(1,i);
            H_eff_y = -M_s*N_d_yy*sin(theta(i))*sin(phi(i))+...
(3*lambda_s/(mu_0*M_s))*sigma(i)*sin(theta(i))*sin(phi(i))+thermal_y(1,i);
            H_eff_z = -
M_s*N_d_zz*cos(theta(i))+thermal_z(1,i)+2*K_s0*cos(theta(i))/(mu_0*M_s*th);

```

```

end

if i <= sttstart || i > (sttstart+stttime+sttfield)
    beta(i) = 0;

elseif i > sttstart && i <= (sttstart+sttbuildup)
    slope = (h_bar*J/(th*M_s*mu_0*e))/(sttbuildup);
    beta(i) = slope*(counting(i)-sttstart);

elseif i > (sttstart+(stttime-stttrampdown)) && i <= (sttstart+stttime)
    slope = (h_bar*J/(th*M_s*mu_0*e))/(stttrampdown);
    beta(i) = -slope*(counting(i)-(sttstart+stttime));

elseif i > (stttime+sttstart) && i <= (stttime+sttstart+sttfield)
    beta(i) = h_bar*Jlow/(th*M_s*mu_0*e);

else
    beta(i) = h_bar*J/(th*M_s*mu_0*e);
end

m_x(i) = -gamma*(H_eff_z*sin(theta(i))*sin(phi(i))...
-H_eff_y*cos(theta(i)))...
-
alpha*gamma*(H_eff_y*sin(theta(i))*cos(phi(i))*sin(theta(i))*sin(phi(i))...
-H_eff_x*(sin(theta(i))*sin(phi(i)))*(sin(theta(i))*sin(phi(i)))...
-H_eff_x*cos(theta(i))*cos(theta(i))...
+H_eff_z*sin(theta(i))*cos(phi(i))*cos(theta(i))...
+gamma*beta(i)*epsilon*(cos(theta(i))*sin(theta(i))*cos(phi(i)));

m_y(i) = -gamma*(H_eff_x*cos(theta(i))...
-H_eff_z*sin(theta(i))*cos(phi(i))...
-alpha*gamma*(H_eff_z*sin(theta(i))*sin(phi(i))*cos(theta(i))...
-H_eff_y*cos(theta(i))*cos(theta(i))...
-H_eff_y*(sin(theta(i))*cos(phi(i)))*(sin(theta(i))*cos(phi(i)))...
+H_eff_x*sin(theta(i))*cos(phi(i))*sin(theta(i))*sin(phi(i))...
+gamma*beta(i)*epsilon*(cos(theta(i))*sin(theta(i))*sin(phi(i)));

m_z(i) = -gamma*(H_eff_y*sin(theta(i))*cos(phi(i))...
-H_eff_x*sin(theta(i))*sin(phi(i))...
-alpha*gamma*(H_eff_x*sin(theta(i))*cos(phi(i))*cos(theta(i))...
-H_eff_z*sin(theta(i))*cos(phi(i))*sin(theta(i))*cos(phi(i))...
-H_eff_z*(sin(theta(i))*sin(phi(i)))*(sin(theta(i))*sin(phi(i)))...
+H_eff_y*sin(theta(i))*sin(phi(i))*cos(theta(i))...
-
gamma*beta(i)*epsilon*(sin(theta(i))*cos(phi(i))*sin(theta(i))*cos(phi(i))...
+sin(theta(i))*sin(phi(i))*sin(theta(i))*sin(phi(i)));

theta(i+1) =
theta(i)+dt*(m_x(i)*cos(phi(i))+m_y(i)*sin(phi(i)))/cos(theta(i));

```



```

    phi(i+1) = phi(i)+dt*(m_y(i)*cos(phi(i))-
m_x(i)*sin(phi(i)))/sin(theta(i));

%%%%%%%%%%%%%%%%%%%%%%%%%%%%%%%%%%%%%%%%%%%%%%%%%%%%%%%%%%%%%%%%%%%%%%%%
% Ignore this if no bias magnet
if i <= stresstime           %Bias Magnet Loop
    %sigma(i) = -5e6*sin(t(i)*1e9);
    H_eff_x1 = bias*(M_s*Omega1/(4*pi*R^3))*(2*sin(theta(i))*...
        cos(phi(i)))-
M_s*N_d_xx1*sin(theta1(i))*cos(phi1(i))+thermal_x1(1,i);
    H_eff_y1 = -bias*(M_s*Omega1/(4*pi*R^3))*(sin(theta(i))*...
        sin(phi(i)))-M_s*N_d_yy1*sin(theta1(i))*sin(phi1(i))+...

(3*lambda_s/(mu_0*M_s))*sigma(i)*sin(theta1(i))*sin(phi1(i))+thermal_y1(1,i);
    H_eff_z1 = -bias*(M_s*Omega1/(4*pi*R^3))*(cos(theta(i)))-...

M_s*N_d_zz1*cos(theta1(i))+thermal_z1(1,i)+2*K_s0*cos(theta(i))/(mu_0*M_s*th);

else
    sigma(i) = 0;

    H_eff_x1 = bias*(M_s*Omega1/(4*pi*R^3))*(2*sin(theta(i))*...
        cos(phi(i)))-
M_s*N_d_xx1*sin(theta1(i))*cos(phi1(i))+thermal_x1(1,i);
    H_eff_y1 = -bias*(M_s*Omega1/(4*pi*R^3))*(sin(theta(i))*...
        sin(phi(i)))-M_s*N_d_yy1*sin(theta1(i))*sin(phi1(i))+...

(3*lambda_s/(mu_0*M_s))*sigma(i)*sin(theta1(i))*sin(phi1(i))+thermal_y1(1,i);
    H_eff_z1 = -bias*(M_s*Omega1/(4*pi*R^3))*(cos(theta(i)))-...

M_s*N_d_zz1*cos(theta1(i))+thermal_z1(1,i)+2*K_s0*cos(theta(i))/(mu_0*M_s*th);
end

m_x1(i) = gamma*(H_eff_z1*sin(theta1(i))*sin(phi1(i))...
    -H_eff_y1*cos(theta1(i)))...
-
alpha*gamma*(H_eff_y1*sin(theta1(i))*cos(phi1(i))*sin(theta1(i))*sin(phi1(i))...
    -H_eff_x1*(sin(theta1(i))*sin(phi1(i)))^(2)...
    -H_eff_x1*cos(theta1(i))^2)...
    +H_eff_z1*sin(theta1(i))*cos(phi1(i))*cos(theta1(i)));

m_y1(i) = gamma*(H_eff_x1*cos(theta1(i))...
    -H_eff_z1*sin(theta1(i))*cos(phi1(i)))...
    -alpha*gamma*(H_eff_z1*sin(theta1(i))*sin(phi1(i))*cos(theta1(i))...
    -H_eff_y1*cos(theta1(i))^2)...
    -H_eff_y1*(sin(theta1(i))*cos(phi1(i)))^(2)...
    +H_eff_x1*sin(theta1(i))*cos(phi1(i))*sin(theta1(i))*sin(phi1(i)));

m_z1(i) = sqrt(1-(m_y1(i)^2+m_x1(i)^2));
%%%%%%%%%%%%%%%%%%%%%%%%%%%%%%%%%%%%%%%%%%%%%%%%%%%%%%%%%%%%%%%%%%%%%%%%

```

```

        theta1(i+1) =
theta1(i)+dt*((m_x1(i)*cos(phi1(i))+m_y1(i)*sin(phi1(i)))/cos(theta1(i)));
        phi1(i+1) = phi1(i)+dt*((m_y1(i)*cos(phi1(i))-
m_x1(i)*sin(phi1(i)))/sin(theta1(i)));
    end

    sigma(i+1) = 0;
    phi = phi*180/pi;
    phi1 = phi1*180/pi;
    theta = theta*180/pi;

    figure(1)
    hold on
    plot (t,abs(theta))
    [pks,locs,w,p] = findpeaks(phi);
    format long

    if freqfind == 1
        period1 = locs(2+dif)-locs(1+dif);
        period2 = locs(3+dif)-locs(2+dif);
        period3 = locs(4+dif)-locs(3+dif);
        period4 = locs(5+dif)-locs(4+dif);
        period5 = locs(6+dif)-locs(5+dif);
        freq(j+1) = 2*1e12/((period1+period2+period3+period4)/4);
    end

    phimax(j,1) = max(phi(1:sttstart));
    phimin(j,1) = min(phi(1:sttstart));

    if max(phi) > 180 || min(phi) < 0
        switching(j) = 1;

    else
        switching(j) = 0;
    end
    if 90 <= theta(end) && theta(end) <= 270
        success(j) = 1;

    elseif -270 <= theta(end) && theta(end) <= -90
        success(j) = 1;

    else
        success(j) = 0;
    end

    thetamax(j,1) = max(theta((sttstart-1000):sttstart));
    thetamin(j,1) = min(theta((sttstart-1000):sttstart));
    avg_final(j,1) = (thetamax(j,1)+thetamin(j,1))/2;
    freq(j+1) = freq(j)+freqdiff;

```

```

end
xlabel('Time (ns)')
ylabel('Angle (deg)')
avg_final;
maxphi = max(phimax);
minphi = min(phimin);
avg_phimax = sum(phimax(:,1))/m;
avg_phimin = sum(phimin(:,1))/m;
best_freq = table(freq(1:j)*10^-9,avg_final);
Highest_Deflection = sortrows(best_freq,2,'descend');
Frequencies = freq(1:j)/2;
switching_chance = sum(switching)/m;
success_chance = sum(success)/m
figure(1)
figure(2)
plot (t,sigma)
figure(3)
plot (t,beta(1:i+1))
toc

```

3. MATLAB code for Figure 2.5(c)

```

clc, clearvars, close all
tic
%%%%%%%%%%%%%%%%%%%%%%%%%%%%%%%%%%%%%%%%%%%%%%%%%%%%%%%%%%%%%%%%%%%%%%%%%%
%CONSTRAINTS
T = 300; % [K] Temperature
sig = 0*100e6; % [MPa] Stress applied in the Y-direction, (-)
           )=compression
frequency = 9.95e9; % [Hz] Stress Frequency
freqdiff = 0.0e9;
sttstart = 8e3; % [ps] Time When STT is Started
stttime = 0.7e3; % [ps] How Long STT is Applied
sttbuidup = 0e3;
sttrampdown = 0e3;
sttfield = 0e3;
rest = 5e3; % [ps] Time at End to Allow Magnets to Rest
tf = (sttstart+stttime+rest)*10^-12; % [s] Run Length
stresstime = sttstart+stttime; % [ps] Applied Stress Time
J = 0*1.6e11;
Jlow = 0*-1.5e11;
P = 0.8;
dif = 6; % Number of peaks to skip when finding average
m = 10000; % Number of simulations to run
bias = 0; % Set to 1 for Bias Magnet
%thermal = 0; % Set to 1 for thermal noise

```

```

freqfind = 0; %Set to 1 to find resonant frequency
%%%%%%%%%%%%%%%%%%%%%%%%%%%%%%%%%%%%%%%%%%%%%%%%%%%%%%%%%%%%%%%%%%%%%%%%
% Constants
mu_0 = 4*pi*10^(-7); %[H/m] Permeability of Free Space
K = 1.3806e-23; %[m^2*kg/(s^2*K)] Boltzmann Constant
h_bar = (6.634e-34)/(2*pi);
e = 1.6e-19;
% Parameters
a = 50e-9; %[m] Major Axis Diameter
b = 50e-9; %[m] Minor Axis Diameter
th = 1.5e-9; %[m] Thickness
Omega = 0.25*pi*a*b*th; %[m^3] Volume
a1 = 102.75e-9; %[m] Major Axis Diameter
b1 = 98.25e-9; %[m] Minor Axis Diameter
th1 = 10e-9; %[m] Thickness
Omega1 = 0.25*pi*a1*b1*th1; %[m^3] Volume
M_s = 0.8e6; %[A/m] Saturation Magnetization
alpha = 0.015; %[-] Gilbert Damping Constant
gamma = 2.2e5; %[-] Gyromagnetic Ratio
lambda_s = 350e-6; %[-] Magnetostriction
R = 200e-9; %[m] Center Distance Between Magnets
% Time
dt = 1e-12; %[s] Time Step
n = int16((tf/dt)+1); %Number of Steps
t = 0:dt:tf+dt;
K_eff = 40*(K*300)/(Omega);
K_s0 = (K_eff+mu_0*M_s^2/2)*th;
phimax = zeros(m,1);
phimin = zeros(m,1);
% Shape Anisotropy
N_d_yy = (pi/4)*(th/a)*(1-(1/4)*((a-b)/a)-(3/16)*((a-b)/a)^2);
N_d_xx = (pi/4)*(th/a)*(1+(5/4)*((a-b)/a)+(21/16)*((a-b)/a)^2);
N_d_zz = 1-(pi/4)*(th/a)*(2+((a-b)/a)+(18/16)*((a-b)/a)^2);
Check = N_d_xx+N_d_yy+N_d_zz; %Check Should = 1
switching = zeros(m,1);
success = zeros(m,1);
barrier = mu_0*M_s^2*(N_d_xx-N_d_yy)/(3*lambda_s);
var = 2*alpha*K*T/(dt*gamma*M_s*Omega*mu_0);
epsilon = P/2;
o = 41;
jj = 4;
for kk = 1:jj

    J = 0;

    if kk == 2
        sig = 30e6
        frequency = 11.36e9;

    elseif kk == 3

```

```

sig = 60e6
frequency = 10.79e9;

elseif kk == 4
sig = 100e6
frequency = 9.95e9;

end
sig
for k = 1:o

parfor j = 1:m

freq = zeros(m,1);
freq(j) = frequency;

beta = zeros(n+1,1);

sigma = zeros(n,1);

theta = zeros(n,1);
phi = zeros(n,1);

m_x = zeros(n,1);
m_y = zeros(n,1);
m_z = zeros(n,1);

%Initial Conditions
theta(1) = 1*pi/180; %89.9*pi/180;    %[rad] (90 is in plane) Polar
Magnetization Angle
phi(1) = 89.84*pi/180;    %[rad] Azimuthal Magnetization Angle

m_y(1) = sin(theta(1))*sin(phi(1));
m_x(1) = sin(theta(1))*cos(phi(1));
m_z(1) = cos(theta(1));

thermal_x = sqrt(var)*randn(1,n);
thermal_y = sqrt(var)*randn(1,n);
thermal_z = sqrt(var)*randn(1,n);

for i = 1:n
counting = zeros(n+1,1);
counting(i) = i;

if i <= stresstime
if T > 0
sigma(i) = -sig*sin(2*pi*t(i)*freq(j));

else
sigma(i) = -sig*sin(2*pi*t(i)*freq(j));

```

```

        end

        H_eff_x = -
M_s*N_d_xx*sin(theta(i))*cos(phi(i))+thermal_x(1,i);
        H_eff_y = -M_s*N_d_yy*sin(theta(i))*sin(phi(i))+...

(3*lambda_s/(mu_0*M_s))*sigma(i)*sin(theta(i))*sin(phi(i))+thermal_y(1,i);
        H_eff_z = -
M_s*N_d_zz*cos(theta(i))+thermal_z(1,i)+2*K_s0*cos(theta(i))/(mu_0*M_s*th);

        else
            sigma(i) = 0;                %Stress applied in the Y-
direction, (-)=compression

            H_eff_x = -
M_s*N_d_xx*sin(theta(i))*cos(phi(i))+thermal_x(1,i);
            H_eff_y = -M_s*N_d_yy*sin(theta(i))*sin(phi(i))+...

(3*lambda_s/(mu_0*M_s))*sigma(i)*sin(theta(i))*sin(phi(i))+thermal_y(1,i);
            H_eff_z = -
M_s*N_d_zz*cos(theta(i))+thermal_z(1,i)+2*K_s0*cos(theta(i))/(mu_0*M_s*th);
        end

        if i <= sttstart || i > (sttstart+stttime+sttfield)
            beta(i) = 0;

        elseif i > sttstart && i <= (sttstart+sttbuildup)
            slope = (h_bar*J/(th*M_s*mu_0*e))/(sttbuildup);
            beta(i) = slope*(counting(i)-sttstart);

        elseif i > (sttstart+(stttime-sttrampdown)) && i <=
(sttstart+stttime)
            slope = (h_bar*J/(th*M_s*mu_0*e))/(sttrampdown);
            beta(i) = -slope*(counting(i)-(sttstart+stttime));

        elseif i > (stttime+sttstart) && i <= (stttime+sttstart+sttfield)
            beta(i) = h_bar*Jlow/(th*M_s*mu_0*e);

        else
            beta(i) = h_bar*J/(th*M_s*mu_0*e);
        end

        m_x(i) = -gamma*(H_eff_z*sin(theta(i))*sin(phi(i))...
-H_eff_y*cos(theta(i)))...
-
alpha*gamma*(H_eff_y*sin(theta(i))*cos(phi(i))*sin(theta(i))*sin(phi(i))...
-
H_eff_x*(sin(theta(i))*sin(phi(i)))*(sin(theta(i))*sin(phi(i)))...
-H_eff_x*cos(theta(i))*cos(theta(i))...
+H_eff_z*sin(theta(i))*cos(phi(i))*cos(theta(i)))...

```

```

+gamma*beta(i)*epsilon*(cos(theta(i))*sin(theta(i))*cos(phi(i)));

        m_y(i) = -gamma*(H_eff_x*cos(theta(i))...
                -H_eff_z*sin(theta(i))*cos(phi(i))...
                -
alpha*gamma*(H_eff_z*sin(theta(i))*sin(phi(i))*cos(theta(i))...
                -H_eff_y*cos(theta(i))*cos(theta(i))...
                -
H_eff_y*(sin(theta(i))*cos(phi(i)))*(sin(theta(i))*cos(phi(i)))...

+H_eff_x*sin(theta(i))*cos(phi(i))*sin(theta(i))*sin(phi(i))...

+gamma*beta(i)*epsilon*(cos(theta(i))*sin(theta(i))*sin(phi(i)));

        m_z(i) = -gamma*(H_eff_y*sin(theta(i))*cos(phi(i))...
                -H_eff_x*sin(theta(i))*sin(phi(i))...
                -
alpha*gamma*(H_eff_x*sin(theta(i))*cos(phi(i))*cos(theta(i))...
                -
H_eff_z*sin(theta(i))*cos(phi(i))*sin(theta(i))*cos(phi(i))...
                -
H_eff_z*(sin(theta(i))*sin(phi(i)))*(sin(theta(i))*sin(phi(i)))...
                +H_eff_y*sin(theta(i))*sin(phi(i))*cos(theta(i))...
                -
gamma*beta(i)*epsilon*(sin(theta(i))*cos(phi(i))*sin(theta(i))*cos(phi(i))...
                +sin(theta(i))*sin(phi(i))*sin(theta(i))*sin(phi(i)));

        theta(i+1) =
theta(i)+dt*(m_x(i)*cos(phi(i))+m_y(i)*sin(phi(i)))/cos(theta(i));
        phi(i+1) = phi(i)+dt*(m_y(i)*cos(phi(i))-
m_x(i)*sin(phi(i)))/sin(theta(i));

    end

    sigma(i+1) = 0;
    phi = phi*180/pi;

    theta = theta*180/pi;

    if 90 <= theta(end) && theta(end) <= 270
        success(j) = 1;

    elseif -270 <= theta(end) && theta(end) <= -90
        success(j) = 1;

    else
        success(j) = 0;
    end
end

```

```
    end
    J
    success_chance = sum(success)/m
    J = J+0.1e11;
end
end
toc
```